CHALMERS

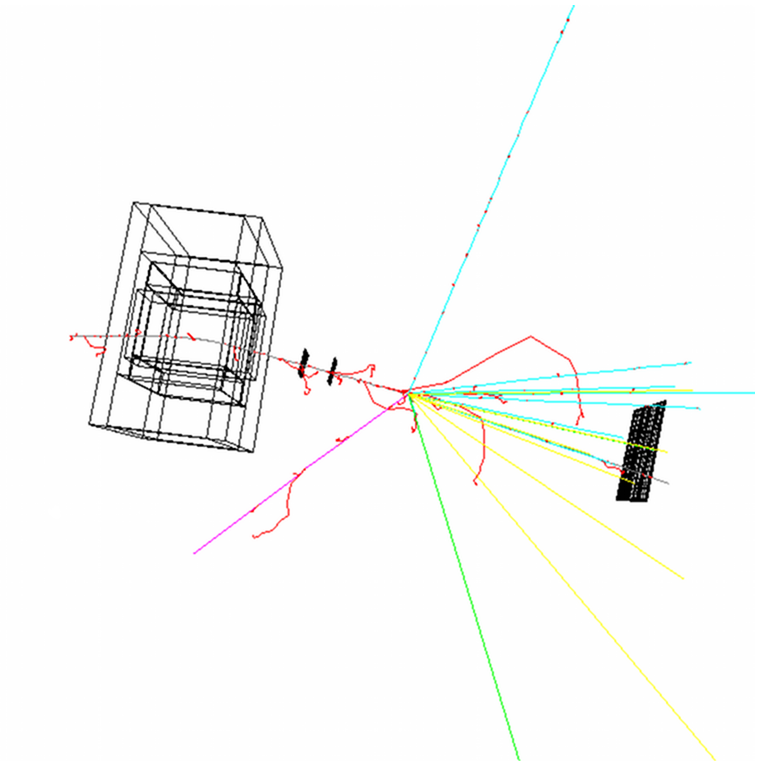

EventGenerators

Master Thesis in Physics and Astronomy

STEFAN BULLER

Department of Fundamental Physics
Chalmers University of Technology
Gothenburg, Sweden 2015

EventGenerators

Master's Thesis

by

Stefan Buller

Supervisors:

Andreas Heinz

Examiners:

??

Department of Fundamental Physics
Chalmers University of Technology
Gothenburg, Sweden 2015

EventGenerators
Stefan Buller (bstefan@student.chalmers.se)

FUFX03 - Master's thesis at Fundamental Physics
Master's Thesis No. FUFX03-15-??

Supervisor: Andreas Heinz
Examiners: ??

Department of Fundamental Physics
Chalmers University of Technology
SE-412 96 Göteborg
Sweden
+46 (31) 772 1000

Printed by Chalmers Reproservice
Göteborg, Sweden 2015

Cover: Describe the cover picture

Abstract

This thesis describes...

Sammandrag

Denna tes beskriver...

Acknowledgements

Thanks to Heinz!

Stefan Buller, Gothenburg, May 2015

Contents

1. Introduction

As a part of the construction of the international FAIR (Facility for Antiproton and Ion Research), the LAND experimental setup will be succeeded by the R^3B (Reactions with Relativistic Radioactive Beams) setup, which includes a score of new detectors. During all stages of this process – from designing and calibrating the new individual detectors and the entire setup, to analyzing the data and extracting the underlying physics – simulations are or will be used.

The R^3B experiment aims to study nuclear physics, in particular the properties of exotic nuclei far from the valley of stability [1]. The experiments will be performed with radioactive beams, and the aim is to be able to determine the complete kinematics of the reaction. We will here describe a generic experiment of this kind.

The radioactive beam impinges on a target surrounded by detectors. In the case of a reaction at the target – a so called *event* – the reaction products are, ideally, identified by recording where they hit the detector, when they hit the detectors (which allows detector output to be attributed to individual events, which yields the initial and final momentum); how much energy they deposit in the detectors (yielding the charge); and their deflection in a magnetic field, which gives their charge-to-mass ratio, and thus their mass.

This is of course a simplification: the reaction products may decay in-flight, they may be deflected by interacting with the air, or a detector. This is why simulations are used, specifically Monte-Carlo simulations, since the underlying physics is non-deterministic.

While simulations are used to determine how a given reaction product propagates throughout the experimental setup, they are not necesarilly needed for the actual reactions at the target, since the purpose of the experiment is to investigate those. In many cases, it is enough to simulate particles with specified initial momenta – matching the kinematic constraints of the reaction – and see how they propagate through the experimental setup, which should be able to identify them even if they are not the result of an actual reaction. However, since the setup in practice only should identify actual reactions products, it would be more ideal if the simulations incorporated some of the theory around the reactions to be studied. Having complete knowledge of the outgoing particle in the simulation may also tempt the user to overestimate the detector efficiency, since they will more easily be able to identify their particle when they know what they are looking for, and when no other processes are involved.

1.1. Event Generator for R^{3}B

As mentioned in the previous section, an experimental event is a reaction between the target and the beam. An *event generator*, on the other hand, is in this context a piece of code that mimics certain reactions for simulation codes. The output of such an event generator would be final state momenta and energies of the reacting particles, which can then be propagated through the simulated experimental setup.

In principle, one can think of an event generator that exactly simulates the reactions at the target and returns a final state with a probability mimic the experiment. However, there are good reasons to not implement this event generator, not all of them related to how unfeasible that project would be – considering our present knowledge of nuclear physics. I will explain this in the next section.

!!!I AM USING 'I' HERE SINCE I BELEIVE THIS TO BE LESS OF AN OBJECTIVE CONCLUSSION. I'M NOT 100% SURE ABOUT THIS USAGE, THOUGH!!!

1.1.1. Design of an Event Generator

An event generator for R^{3}B needs to have certain features, that may be more or less important for more general purpose event generators. Firstly, it does not need to reproduce every feature of the experimental spectra, as long as it gives the general features. The actual experiment will determine the details. On the other hand, it needs to be easy to change the underlying model and see how this influences the resulting spectra, since quantities in the model – nuclear level densities, transition rates, etc. – are influenced by the presence of phenomenon the experimenters are actually interested in finding – such as giant resonances or halo structures – that is not directly observable in the experimental data. It should also be possible to steer the event generator to generate certain reactions, that are experimentally distinguishable, so that the event generator could be used to evaluate the detector efficiency for such reactions.

2. Theoretical Background

2.1. Nuclear Collisions

From a macroscopic perspective, nuclei can be viewed as charged particles, and thus collisions (here in a loose sense) between them is essentially governed by the Rutherford scattering formula. This is how the nucleus was discovered in the first place. However, this simple picture breaks down at higher energies, when the de Broglie wave-length ($\lambda \sim \boldsymbol{p}^{-1}$) becomes sufficiently small to resolve the inner structure of the nuclei. At even higher energies, it becomes feasible to model the collision as not taking place between the two nuclei, but by individual protons and neutrons (nucleons).

This leads us to the *participant-spectator* picture of nuclear collisions, in which the collision is viewed as if taking place between a few *participant* nucleons, while the remaining *spectator* nucleons remain mostly unaffected. Such a reaction is known as *quasi-elastic scattering*, since the kinetic energy of the projectile will be much greater than the binding energy of the participants, which further motivates treating them as approximately free particles, and means that the kinetic energy will almost be conserved, hence *quasi-elastic*. !!!POSSIBLY DISCUSS LIMITATIONS!!! The collision between the participant nucleons takes place at a time scale of about 10^{-23} s [2], and is sometimes called a *fireball* or *firestreak*.

However, this is just the first part of the collision. The participant nucleons may have gone unaffected through it, but the resulting system (a so-called pre-fragment) will be highly excited, and will decay to the actual fragment – often by ejecting nucleons, in this context known as evaporating them. The characteristic time-scale for these ejections vary between 10^{-21} – 10^{-16} s, depending on the energies and emitted particle [2].

In this picture, we thus have a two-step process to describe nuclear fragmentation. Various models to describe both steps exist in the literature, which can be combined more or less freely—they do not necesarilly use the same paremeters to describe the nuclues. Models which mainly use parameters like A, the number of nucleons, Z the number of protons, the total nuclear-spin J and the excitation energy E of the nucleus are termed *macroscopic*, while models that directly treat the states of individual nucleons are called *microscopic*. Examples of the former are the *abrasion-ablation model* [3], while the *intranuclear-cascade model* [4] is an example of a microscopic model. As is often the case in nuclear physics, no one model is valid of all range of nucleon number A and incident energies [5].

Since the focus on this report is to describe an event-generator for a physics experiment, we do not need a state of the art model (see !!!AUTOREF TO SECTION!!! for the arguments). Since the macroscopic properties of nuclei are more easily related to expermental observables, we will restrict our attention to those.

2.1.1. The fast processes – the Goldhaber model

!!! SUDDENLY, CODE. INTRODUCE MODEL FIRST? !!! To mimic existing code !!!CITE LEONID?!!! and to allow the user to study a reaction of their interest, the outcome of the first stage of the process is largely determined by user input: the participant projectile nucleons – the cluster – as well as its invariant mass, and the excitation energy of the pre-fragment are both specified by user input. The only specific model used is to determine the momentum of the participant system relative to the projectile, everything else is just conservation of momentum, and an isotropic cross-section. The *Goldhaber model* states that the momentum distribution is given by a Guassian with the width determined by the expectation value of the momentum of an individual nucleon, explicitly

$$\sigma^2 = \langle \boldsymbol{p}^2 \rangle A \frac{A_\mathrm{p} - A}{A_\mathrm{p} - 1}, \tag{2.1}$$

where A_p is the number of nucleons in the projectile, A in the pre-fragment, and $\langle \boldsymbol{p}^2 \rangle$ is the expectation value of the momentum of an individual nucleon. For a Fermi-gas, $\langle \boldsymbol{p}^2 \rangle$ may be written in terms of the Fermi-momentum $\boldsymbol{p}_f$ as $\frac{3}{5}\boldsymbol{p}_f^2$ [6]. !!!THIS IS NOT THE MODEL USED IN LEONID CODE!!!

!!!LEONID USES

$$\sigma^2 = 2(M + m - M_p)\frac{mM}{m+M} = 2Q\mu(m,M),$$

where m is the mass of the participant, M_p the mass of the projectile and M the mass of the pre-fragment. If we take $Q = T = mv^2/2$, we get $\sigma^2 = m^2v^2$, which could imply that this is just the Fermi-momentum? !!!

!!!POSSIBLY MOVE NEXT TO CODE DOCUMENTATION, SINCE WHICH FRAME WE USE WHERE IS NOT REALLY GENERAL THEORY!!! Momentum conservation implies that

$$p_\mathrm{p} = p_\mathrm{i} + q_\mathrm{pf} \tag{2.2}$$

$$p_\mathrm{i} + p_\mathrm{t} = q_\mathrm{i} + q_\mathrm{t} \tag{2.3}$$

where p_p is the 4-momenum of the projectile, p_t the momentum of the target, p_i the internal momentum of the cluster; q_pf the final momenum of the pre-fragment q_i and q_t the final momentum of the target and cluster, respectively.

Solving the above equation and squaring for p_i and squaring gives an expression for the off-shell mass of the cluster as

$$p_\mathrm{i}^2 = p_\mathrm{p}^2 + q_\mathrm{pf}^2 - p_\mathrm{p} \cdot q_\mathrm{pf} = m_\mathrm{i}^2 = M_\mathrm{p}^2 + M_\mathrm{pf}^2 - M_\mathrm{p}\sqrt{M_\mathrm{pf} + \boldsymbol{p}_i^2}, \tag{2.4}$$

where we have evaluated $p_\mathrm{p} \cdot q_\mathrm{pf}$ in the rest-frame of the pre-fragment.

Since we are interested in constructing an event generator, we next transform the cluster's 4-momentum from the projectile to the laboratory frame (the projectile and target momentum is already known in the laboratory frame, the former being zero practically being a definition of that frame). The relevant gamma factor is $\gamma = 1+T/m_\mathrm{p}$, where T is the kinetic energy of the projectile.

Since the collision between the target and the cluster is easier to do in their zero-momentum (ZM) frame, we also need to transform between the laboratory and that frame. This is readily done by noting

$$\bar{\boldsymbol{P}} = \boldsymbol{p}_i + \boldsymbol{p}_t = \gamma(\beta_\mathrm{ZM})\bar{m}\beta_\mathrm{ZM} = \bar{E}\beta_\mathrm{ZM} \implies \beta_\mathrm{ZM} = (\boldsymbol{p}_i + \boldsymbol{p}_t)/\bar{E}, \tag{2.5}$$

where $\bar{E}$ etc. denotes the energy of the system of both particles. Since we want the β between the lab and the ZM frame, we evaluate all the quantities in the lab frame

$$\beta_\mathrm{ZM} = \frac{\boldsymbol{p}_i}{E_\mathrm{c} + m_\mathrm{t}}. \tag{2.6}$$

The scattering between target and cluster is back-to-back in the ZM frame, and we generate the scattering angle from an isotropic $\frac{d\sigma}{dt}$, which in practice means that the Mandelstam variable t is a uniform random number. The ZM energy, momentum and scattering angle can be readily expressed in term of the invariant Mandelstam variables

$$E_\mathrm{c} = \frac{s + m_\mathrm{i} - m_\mathrm{t}}{2\sqrt{s}} \tag{2.7}$$

$$|\boldsymbol{p}_\mathrm{c}| = \sqrt{E_\mathrm{c}^2 - m_\mathrm{i}^2} \tag{2.8}$$

$$\cos\theta = \frac{t - m_\mathrm{i}^2 - m_\mathrm{c}^2 + 2E_\mathrm{c}^2}{2|\boldsymbol{p}_\mathrm{c}|^2}. \tag{2.9}$$

A random polar angle ϕ in [0,2π] is then generated, which together with $|\boldsymbol{p}_\mathrm{c}|$, θ and E_c fix the ZM 4-momentum of the cluster, and also the target by $\boldsymbol{p}_\mathrm{t} = -\boldsymbol{p}_\mathrm{c}$. Using (2.6), these results are boosted to the lab frame, in which we now have an expression for all the relevant momenta.

2.1.2. The slow process – decay of a compound nucleus

There are at least two models for the decay of a compound nucleus popular in the literature, the Hauser-Feshbach and the Ewing-Weisskopf formulas. Both aim to describe how a compound nucleus in a given macro-state ($E*$, J, Z, A) will decay.

The older Ewing-Weisskopf formula, which this work is based on, gives the probability of decaying by evaporating a particle ν as

$$\frac{d^2P_\nu}{dE_f dt} = \frac{1}{\hbar}\frac{\rho(E_f,J_f)}{\rho(E_i,J_i)} \sum_{S=|J_f-s|}^{|J_f+s|} \sum_{l=|J_i-S|}^{|J_i+S|} T_l(\epsilon_\nu), \qquad [7] \tag{2.10}$$

where P is the probability, E_f the final-state energy, J_f the final-state spin, ρ the level densities and

$$\epsilon_\nu \approx E_f - E_i - S_\nu \tag{2.11}$$

the kinetic energy of the evaporated particle, S_ν being its separation energy $S_\nu = M_f + m_\nu - M_i$[1] . s is the intrinsic spin of the evaporated particle, S is the spin of the system consisting of the final state nucleus and evaporated particle, with l being the orbital angular momentum of that state with respect to its center of mass. The sums give all the way to couple these while conserving the total angular momentum $\boldsymbol{J}_f + \boldsymbol{s} + \boldsymbol{l} = \boldsymbol{S} + \boldsymbol{l} = \boldsymbol{J}_i$. T_l is the transition probability. By integrating over E, we get $\frac{dP_\nu}{dt} = \Gamma_\nu$, which is roughly proportional to the probability to decay through the channel ν, $P_\nu = \Gamma_\nu / \Gamma_{\text{tot}}$.

Provided that the characteristic life-time of the system is short compared to the time resolution of the experimental setup, we may essentially treat the decay-widths as probabilities, since – as far as the experiment is concerned – the decay may as well take place instantenously. Note that the system may undergo multiple decays before it reaches its ground-state, and that time-scale of this entire decay chain must be short by the experimental standards. The time-of-flight resolution of the future R^{3}B setup will be in the picosecond range (10^{-12} s) [1], which is well above the time-scales of single evaporation given by Gaimard and Schmidt (10^{-21} – 10^{-16} s) [2]. Hence we will view Γ_x as the probability to decay by a given process in an unspecified but short time step.

Since we are interested in simulating a decay chain, we want more information than merely the probability to decay by emitting a specific particle. We thus take a step back from (2.12), and undo the summation over l

$$\frac{d\Gamma_{\nu,l}}{dE_f} = \frac{1}{\hbar}\frac{\rho(E_f,J_f)}{\rho(E_i,J_i)} \sum_{S=|J_f-s|}^{|J_f+s|} T_l(\epsilon_\nu), \tag{2.12}$$

which finally gives us the decay probability (per unit energy) from an initial state (E_i,J_i) to a final state (E_f,J_f) by emmiting a particle ν with angular momentum l and momentum given by conservation of energy.

ν can in principle be any particles. However, the photon must be treated differently as it is massless and thus fully relativistic – which makes the dististinction between l and the intrinsic spin unnatural – and removes a polarization state. With this in mind, we get

$$\frac{d\Gamma_\gamma}{dE_f} = \frac{1}{\hbar}\frac{\rho(E_f,J_f)}{\rho(E_i,J_i)} \sum_{l=|J_f-J_i|}^{|J_f+J_i|} T_l(\epsilon_\gamma) \tag{2.13}$$

$$\Longrightarrow \frac{d\Gamma_{\gamma,l}}{dE_f} = \frac{1}{\hbar}\frac{\rho(E_f,J_f)}{\rho(E_i,J_i)} T_l(\epsilon_\gamma), \tag{2.14}$$

[1] The approximation is due to neglecting the kinetic energy of the daughter nucleus, which should be a good approximation when the evaporated particle ν is light. This is not a necesary approximation, though, and a more exact formula is presented in !!!autoref!!!. The separation energy does not enter as a cost of removing the particle ν, but rather to relate the two excitation energies E_f and E_i to an absolute scale.

where $l > 0$ is an integer.

Although ν could be any particle, it becomes more appropriate to model the decay as a fission process if ν becomes sufficiently heavy in relation to the compound nucleus. Fission is usual modeled as a transition first to a *transition state*, beyond which the nucleus will inevitably fission [8]. The present work does not include fission, and we will thus not discuss its details here. Swiateck discussed the possibility of treating particle emission and fission in an essentially symmetric fashion, by using a transition state formalism also for lighter particles [9]. !!MAY BE INTERESTING TO SAY SOMETHING ABOUT THIS. FIND SOURCE ON WHY THIS APPROACH ISN'T USED.!!

We will now describe models for the level density ρ and transition probability T_l.

Level densities

The level density $\rho(E,J)$ enumerates the number of energy levels of a given nucleus in an energy range $[E,E+dE]$ with a given spin J. We have in our notation supressed the dependence on A and Z. The nuclear level density increases rapidly with energy, which suggests that the nuclear levels are not simply built up by exciting single nucleons in a shell-model, since the spacing of these levels do not decrease nearly fast enough.

To see how the rapid increase in level densities may be accounted for by collective excitations, and to introduce some of the terminology, it is illustrative to have a look at a simple example.

The simple example Consider a "nucleus" in which we have A identical nucleons, that occupy single particle states with spacing d. The situation is illustrated in Figure 2.1. The energy of the nuclues is given by

$$E = \sum_i \epsilon_i n_i, \tag{2.15}$$

where $\epsilon = id$ is the energy of level i, and n_i is the occupation number of that level, which can be 0 or 1, since nucleons are fermions. If we take the Fermi energy as the reference energy, we get the excitation energy

$$E^* = \sum_i \epsilon_i n_i - \sum_i^A \epsilon_i n_i. \tag{2.16}$$

The picture is more illustrative than the formulas. We now have one way to excite our system to $E^* = d$, namely by exciting the nucleon just below the Fermi level. For $E^* = 2d$ we may proceed from our $E^* = d$ system in two ways, either by further exciting the lone excited nucleon $E^* = 2d$, or by exciting the highest nucleon in the $A-1$ system, $E^* = d + d$. For $E^* = 3d$, we have

$$\begin{aligned} 1d + 1d + 1d \\ 2d + 1 \\ 3d, \end{aligned} \tag{2.17}$$

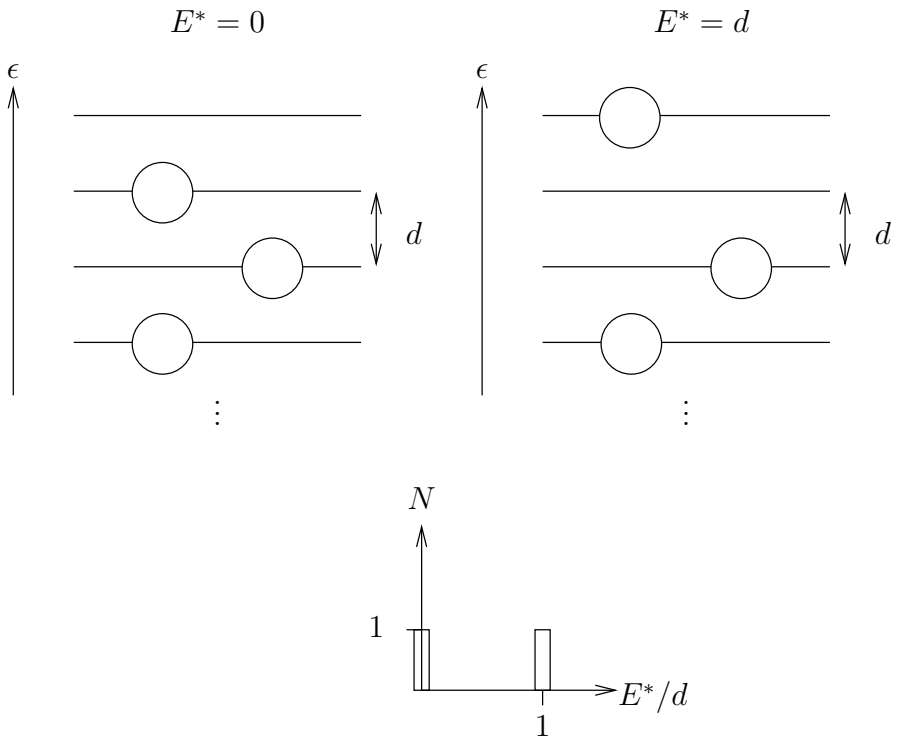

Figure 2.1.: *Fermions with equidistant single-particle levels.*

and at this point, it should be apparent that we are really investigating the number of ways to write a natural number as a sum of natural numbers, a problem which engaged Euler as early as 1720 [10]. It turns out to be a very rapidly growing function, with the number of ways to partition 100 being 190569292 [10].

!!!TODO: mention g=1/d and its relation to a. Smearing out producedur by Laplace+saddle-point. Mention level vs density of states. !!!

Since the level density increases very rapidly, it is reasonable to approximate it as a continuous function for energies above the threshold for particle evaporation. We use the following expression

$$\rho(E,J) = \frac{1}{\sqrt{2}24}\frac{1}{\sigma a^{1/4}U^{5/4}}\exp\left(2\sqrt{aU}\right)\frac{2J+1}{\Theta_{\text{eff}}/(\hbar^2\beta)}\ exp\Big(-(J+\tfrac{1}{2})^2/(2\Theta_{\text{eff}}/(\hbar^2\beta))\Big), \tag{2.18}$$

which is a version of the widely-used expression for the level density of a *Fermi gas* that takes angular momentum J into account [11].

Here, U is an effective excitation energy above the *yrast line*, corrected for shell and pairing effects. It is given by

$$U = E_{\text{eff}} + f(E_{\text{eff}})\delta S + g(E_{\text{eff}})\delta P, \tag{2.19}$$

where f and g describes the damping of shell and pairing effects with increased energy, and $E_{\text{eff}} = E^* - E_{\text{yrast}}$. The *yrast energy* is the lowest energy for a given angular

momentum, here taken to be

$$E_{\text{yrast}} = \frac{(2J+1)\hbar^2}{2\Theta_\perp}, \tag{2.20}$$

corresponding to a quantum-mechanical axi-symmetric rotor rotating around its symmetry axis. This yrast energy is not strictly speaking the lowest energy for a given J, but the energy of a collective rotational excitation, which is a reasonable picture when we have many states with a given J in our energy interval $[E,E+dE]$, which is needed for (2.18) to be valid. !!CITE. THIS IS A GUESS OF MINE. ALSO NOTE THAT THIS IS NOT AN ADDITIONAL ROTATIONAL DOF, SEE NUCLEAR STRUCTURE II BY BOHR + MOTTELSON.!!

The pairing energy δP in (2.19) can be estimated from the average separation energy for the surrounding nuclei (in an (N,Z) plot, like an isotope chart), which is close to the actual observed shift between odd and even nuclei [12]. Neutrons and protons have different pairing energies, which is to be added or subtracted when neutron or proton number, respectively, is odd or even. The shell energy δS can either be calculated from a microscopic model, or – as I have done – can be be estimated together with the pairing energy by comparing experimental masses with masses predicted by a macroscopic model, and taking the difference, as suggested by Schmidt and Morawek [7]. I used the macroscopic part of the 1992 edition of the Finite-Range Droplet Model (FRDM-1992) [13], which is presented in more detail in section 2.2.

The damping of shell effects with energy can be described by an exponential function

$$f(E_{\text{eff}}) = 1 - \exp\left(-E_{\text{eff}}/E_{\text{d}}\right), \tag{2.21}$$

where E_{d} is the shell-damping energy

$$E_{\text{d}} = \frac{0.4}{a}A^{4/3}, \tag{2.22}$$

where a is the level-density parameter, which for a spherical nuclei can be approximated by

$$a = \frac{A}{14.61\,\text{MeV}}(1 + 3.114A^{-1/3} + 5.626A^{-2/3}). \qquad [7] \tag{2.23}$$

This parameter also enters directly into (2.18).

Likewise, the damping of pairing effects with energy can also be described by a simple function, in this case

$$g(E_{\text{eff}}) = \begin{cases} 1 - (1 - E/E_{\text{c}})^2 & E_{\text{eff}} < E_{\text{c}} \\ 1 & E_{\text{eff}} \geq E_{\text{c}}. \qquad [7] \end{cases} \tag{2.24}$$

The critical energy E_{c} is approximately 10 MeV and varies with angular momentum,

$$E_{\text{c}} = 10\,\text{MeV}\sqrt{1 - (J/J_{\text{c}})^2}\,, \tag{2.25}$$

where the critical angular momentum J_{c} is about $12\hbar$. !!!SOURCE FOR THIS?!!!

Since we have restricted ourselves to spherical nuclei in (2.23), we also have the moments of inertia $\Theta_\perp = \Theta_\parallel$. In particular, for a sphere with constant density, we have

$$\Theta = \frac{2}{5} M R_0^2 \approx \frac{2}{5} A^{5/3} \times u \times r_0^2 \tag{2.26}$$

The approximation is obtained by inserting $R_0 = r_0 A^{1/3}$ and $M = uA$, where $r_0 = 1.16\,\text{fm}$ is the nuclear radius constant, with the same value as in the macroscopic model [13]. u is the atomic mass units, $u \approx 931.5\,\text{MeV}$.

Finally, β in (2.18) is the reciprocal nuclear temperature $\beta = 1/T$[2]. It can be calculated from $\frac{a}{\beta}$, which is obtained by solving

$$a/\beta = \sqrt{(aU)[1 - exp{-a/\beta}]}, \qquad [14] \tag{2.27}$$

which can be done numerically by iterating

$$(a/\beta)_{n+1} = \sqrt{aU[1 - exp{-(a/\beta)_n}]} \tag{2.28}$$

from a suitable initial guess $(a/\beta)_0$. $(a/\beta)_0 = \sqrt{aU}$ was used here, which solves (2.27) for $(a/\beta) \to \infty$ and is known to be a good initial guess [14].

In order to get a picture of how all of this comes together, we have plotted the level density for the $A = 10$ isobar for $J = 0, \frac{1}{2}, \ldots, 4$. The level density of ^{20}Ne for different spin with and without subtracting the yrasy-energy is illustrated in Figure 2.2. As can be seen in the figure, the level densities for higher spin start at a lower value for low energies, way lower than 1 level each MeV – which indicates that the continous view of energy levels fails at these energies. The spins appear to be split up in 2 groups, one for $J \leq 1$ and one for $J > 1$. The level densities for $4 \geq J > 1$ initially grow rapidly, until they overtake the lower spin level densities and settle at a seemingly proportional relationship with each other. As a result of the $(2J + 1)\exp(J(J + 1))$ dependence on J, moderate J values give the largest level density. The same general behaviour is seen for the other nuclei at the $A = 10$ isobar.

In order to see if this is a general feature of our model, we also investigate ^{99}Zr – this nuclei being chosen arbitrarily as something far form the $A = 10$ isobar. The corresponding plots of the level densities are seen in Figure 2.3. We note that the inclusion of the yrast energy is not nearly as significant for the spins under consideration, since the larger value of Θ reduces the yrast energy of a given J. This also explains why $J = 4$ has the highest density of states in this case: a higher Θ means that the $\exp(J(J + 1)/\Theta)$ factor does not supress the level density as rapidly with increasing spin. We also see that it is only for $J \geq 3$ that we see the hint of a dip for lower energies. This could perhaps indicate that the pronounced spin-dependence seen for the $A = 10$ isobar will reveal itself for yet higher spin – a natural consequence of the higher moment of inertia for heavier nuclei.

[2] It really is the reciprocal temperature at the saddle-point, see e.g. Feldmeier [14].

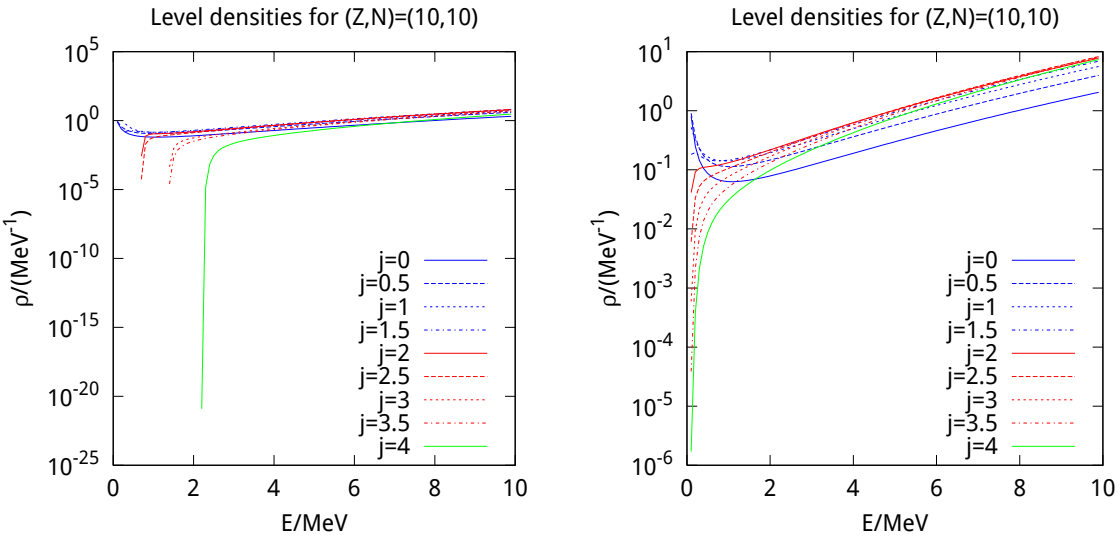

(a) The level densities derived from (2.18).

(b) Without compensating for the yrast energy.

Figure 2.2.: *The energy dependence of the level density of* ^{20}Ne *for spin* $J = 0, \frac{1}{2}, \ldots, 4$. *In order to more easily be able to compare level densities for different spin at the same effective energy above the yrast line, the yrast energy has not been subtracted from* E_{eff} *in* 2.2b.

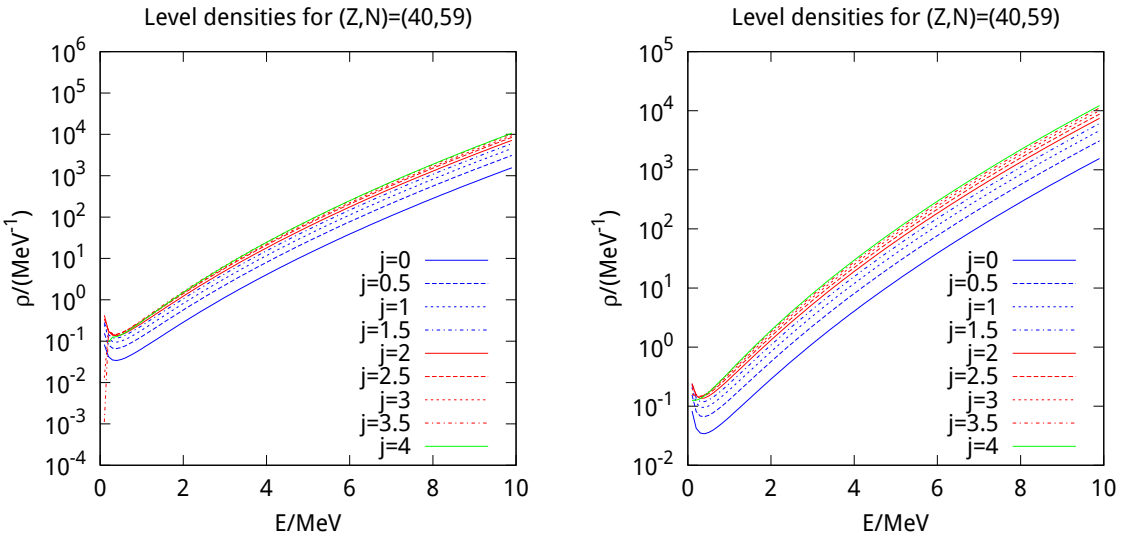

(a) The level densities derived from (2.18).

(b) Without compensating for the yrast energy.

Figure 2.3.: *The energy dependence of the level density of* ^{99}Zr *for spin* $J = 0, \frac{1}{2}, \ldots, 4$. *In order to more easily be able to compare level densities for different spin at the same effective energy above the yrast line, the yrast energy has not been subtracted from* E_{eff} *in* 2.3b.

In any case, this is low-energy behaviour, and both the Fermi gas model [14] and the very notion of a continuous level density has problems for low energies. Most notably, the Fermi gas model itself, without compensating for shell and pairing effects, predicts a singularity at $U = 0$, which is why we see an increase in the level density for lower energies and spin in both Figure 2.3 and Figure 2.2, which have been truncated at $E = 0.1\,\mathrm{MeV}$ in order to avoid this.

The level density was also investigated for a fixed spin for different nuclei on the $A = 10$ isobar, but nothing conclusive was found.

On the other hand, for the isotope $Z = 10$, the level density for higher energies generally increases with additional neutrons, which is to be expected, since there are more ways to arrange the nucleons for a give excitation energy, this is illustrated in Figure 2.4, where the brighter lines correspond to heavier nuclei.

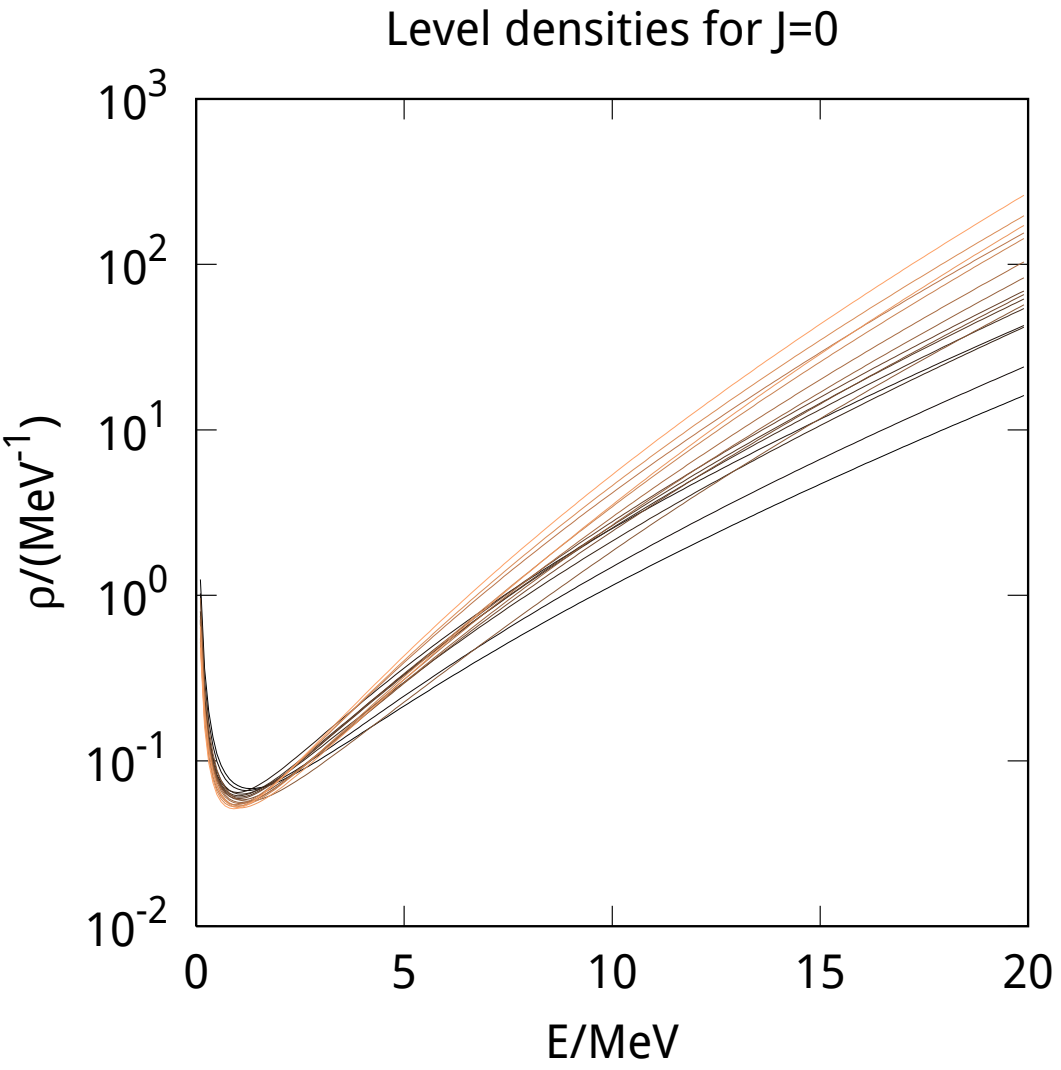

Figure 2.4.: *The level densities for* ^{17}Mg *to* ^{32}Mg*, where brigther lines correspond to heavier nuclei.*

Transition Probabilities

The decay width $\Gamma_{\nu,l}$ into a given final energy interval $[E_f,E_f + dE]$ by particle ν with orbital angular orbital momentum l also depends on the transition probability $T_l(\epsilon_\nu)$.

One of the more well-known models of a transition probability by particle decay is the Gamow model for alpha decay, in which the mother nucleus (Z,N) is modeled as essentially being composed of a ready-to-go alpha particle and the daughter nucleus $(Z-2,N-2)$ and the probability to decay is essentially given by the probability for the alpha particle to tunnel through the potential due to the daughter nucleus, with an additional factor depending on how often the alpha particle has a chance to tunnel.

This model is readily generalized to other particle decays: we may just as well imagine a proton being formed inside the mother nucleus (Z,N), and tunneling through the potential from the daughter nucleus $(Z-1,N)$.

In order to make this model quantitative, we need an actual potential. Approximating the charge distribution of the daughter and tunneling particle as spherical, we may model the potential due to electrostatic interaction as a simple Coulomb potential, which gives us

$$V = V_{\text{Col}} + \cdots = Z_1 Z_2 \frac{e^2}{r_{12}} + \ldots, \tag{2.29}$$

in non-rationalized units. If we go ahead and assume that not only the charge distribution, but the potential as a whole is spherically symmetric, we can employ the standard procedure of splitting up the problem into a radial and angular part, where the radial potential is given by

$$V_{\text{r}} = Z_1 Z_2 \frac{e^2}{r_{12}} + \frac{l(l+1)\hbar^2}{2\mu r^2} + \ldots \tag{2.30}$$

where we still need additional terms to take into account the effective nucleon-nucleon intraction. The assumption of spherical symmetry also gives us the angular part of the wave function as a spherical harmonic, which gives us the angular distribution of the emitted particle in the center-of-mass frame.

The nuclear part of the potential used by CODEX is a proximity potential [15] [16]. Proximity potentials may be derived from a more general approximation method, in which two nearby surface are split up into parallel surface, close enough to be approximated as semi-infinite, see Figure 2.5 [17]. The contributions from these different set of parallel surfaces are assumed to be additive. The potential energy is calculated for these slabs, and factors to correct for the actual geometry are introduced. This approach is widely used in Casimir force calculations between objects of a more arbitrary shape [18]. This approximation is also known by "Derjaguin approximation" in other fields [17].

In the nuclear case, the situation is somewhat complicated by the fact that the form of the nucleon-nucleon interaction is unknown. As such, there exist several proximity potentials [19]. Dutt et. al. showed that 12 common proximity potentials all were able to predict fusion barrier heights with 10% of the experimental values for asymmetric fusion reactions ranging from $^{12}\text{C} + {}^{17}\text{O}$ to $^{86}\text{Kr} + {}^{208}\text{Pb}$ [19]. Proximity-type potentials have also been used to explore alpha and proton decay [20] [21], which is closer to our

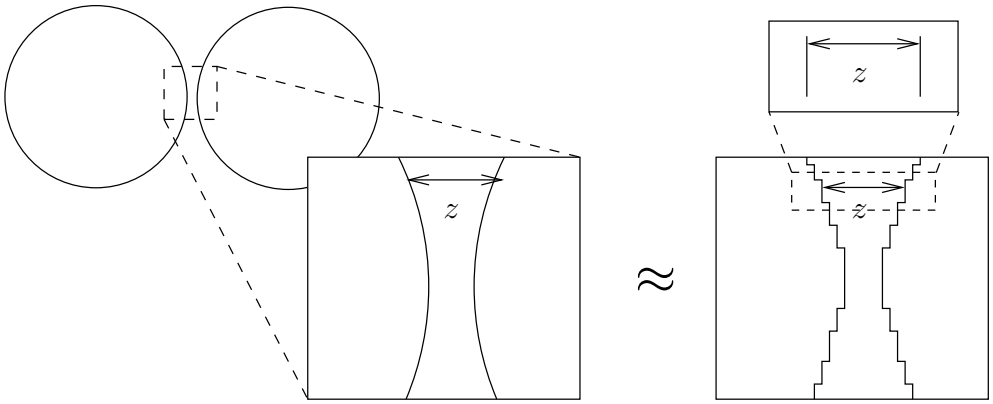

Figure 2.5.: *A schematic sketch of how the proximity approximation is carried out. Two close surfaces are approximated as a series of parallel surface, which in turn are approximated as infinite parallel surface, for which the potential energy is easier to calculate. This result is then summed up for all parallel surfaces.*

intended application[3].

The proximity potential is given by

$$V_{\mathrm{N}} = C\phi(\zeta), \tag{2.31}$$

where $\phi(\zeta)$ is the so-called *universal function*, which for a given nucleon-nucleon interaction is independent of the geometry of the nuclei in the proximity approximation. ζ is a unitless distance between the two nuclei, see below. Geometrical factors are contained in the proportionality "constant" C, which is given by

$$C = 4\pi\gamma b \frac{r_{c,1} r_{c,2}}{r_{c,1} + r_{c,2}} \tag{2.32}$$

where γ is the surface energy coefficient, which can be approximated by

$$\gamma = 0.9517(1.0 - 1.78260 \times I^2), \tag{2.33}$$

where $I = (N - Z)/A$ is the neutron excess.

We use the universal function due to Blocki 1997

$$\phi(\zeta) = \begin{cases} -0.5(\zeta - 2.54)^2 - 0.0852(\zeta - 2.54)^3 & \zeta < 1.2511 \\ -3.437 \exp\left(-\zeta/0.75\right) & \zeta > 1.2511. \qquad [16] \end{cases} \tag{2.34}$$

[3]It is not immediately obvious to the author if the assumptions of the proximity potential formalism applies to proton or alpha decay. It does however reproduce experimental half-lives to a reasonable degree, see e.g. Balasubramaniam and Arunachala [20] – this is for emission from heavier nuclei, though.

ζ is the distance between the two nuclear surfaces, normalized with respect to the typical surface diffuseness of the nuclei, here taken to be 1 fm [16]. More explicitly, we have

$$\zeta = \frac{r - r_{\text{sum}}}{b}, \tag{2.35}$$

where b is the surface diffuseness, and r_{sum} is roughly the sum of the radii of the two nuclei, so that $r - r_{\text{sum}}$ gives the distance between the nuclear surfaces [16]. An effective sharp nuclear surface may be estimated by the formula

$$r_{\text{sharp}} = 1.28A^{1/3} - 0.76 + 0.8A^{-1/3} \quad fm. \qquad [16] \tag{2.36}$$

(2.36) is used to estimate the radii of all nuclei, and as a result $r_{\text{sharp}} = 1.32\,\text{fm}$ for protons and neutrons, which is slightly different from the value of r_0 that is normaly used. In the proximity potential, it is preferable to use the *central radius* r_{c} rather than the effective sharp radius [16], which is given by

$$r_{\text{c}} = r_{\text{sharp}} \left(1 - (br_{\text{sharp}})^2\right) \quad . \qquad [22] \tag{2.37}$$

Hence, $r_{\text{sum}} = r_{\text{c},1} + r_{\text{c},2}$.

Since the proximity model takes the spartial extent of the nuclei into account, we modify the Coloumb-interaction accordingly, from that of a point particle to that of a homogenously charged ball

$$V_{\text{C}} = \begin{cases} \frac{Z_1 Z_2 e^2}{r} & r > r_{\text{ch}} \\ \frac{Z_1 Z_2 e^2}{r_{\text{ch}}^2}(3 - (r/r_{\text{ch}})^2) & r < r_{\text{ch}}, \end{cases} \tag{2.38}$$

where we here use the more common formula for the charge radius, $r_{\text{ch}} = r_0 A^{1/3}$.

We illustrate this total potential in Figure 2.6 ^{20}Ne for tunneling of protons and neutrons. The individual contributions to the total potential may be discerned by looking at the potential for the emission of $l = 0$ neutrons (which are only affected by the proximity potential) and $l = 0$ protons (which have to tunnel through the sum of the Coulomb and proximity potential). On this energy scale, the barrier protons have to tunnel through is merely 2 MeV high, but since the proton separation energy for ^{20}Ne 12 MeV, it will only happen for high excitation energies.

We also see that the centrifugal part quickly dominates, essentially a result of protons and neutrons being relatively light particles: for α-decay, the centrifugal part is about a fourth of the values displayed above, and the l dependence of the tunneling probability is not very significant [23]. This strong l dependence makes proton radioactivity a sensitive probe to the orbital angular momentum of valence protons for proton emitting nuclei [20], but – in this case – it also poses a problem, since it removes the Coulomb+proximity barrier for high l-values. Even for moderate l values, it makes particles with low energy classically forbidden inside the barrier, which appears inconsistent with the picture of a particle tunneling through a barrier. The solution adopted in this work is to assign probability zero to tunnel for particles that are classically forbidden within the nucleus. This will supress decay for higher l, since the bottom of the potential well rises as l does.

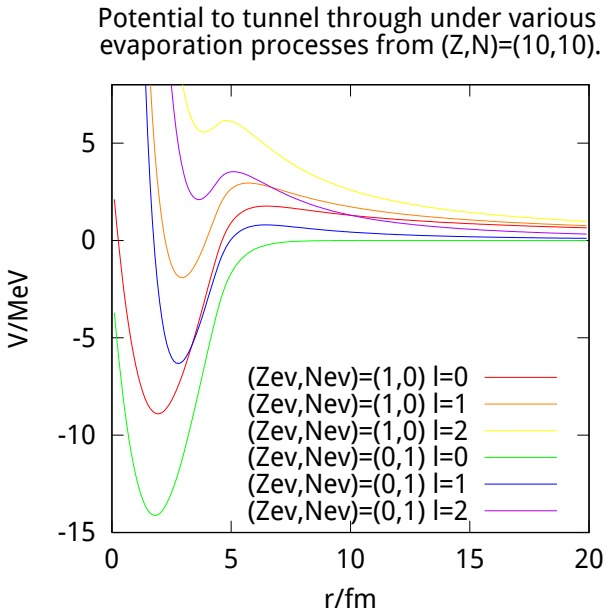

Figure 2.6.: *The potential used for tunneling of neutrons and protons with* $l = 0,1,2$ *from* ^{20}Ne. *The potential for* $l = 0$ *neutrons is exactly the proximity potential* (2.34), *while the* $l = 0$ *proton's potential show the sum of the proximity and Coulomb potential.*

Given the potential, the transition probability can be calculated in the WKB approximation as

$$T_l(\epsilon_\nu) = \exp(-2G), \qquad [8] \tag{2.39}$$

where

$$G = \sqrt{\frac{2\hbar}{\mu}} \int_{r_1}^{r_2} \sqrt{V_l(r) - \epsilon_\nu}\, dr. \tag{2.40}$$

r_1 and r_2 are the inner and outer radii for which the kinetic energy is equal to the potential energy. It should be noted that the WKB approximation is not strictly speaking valid for regions where the potential is approximately constant over several wave-lengths $\lambda = \frac{2\pi}{k}$, which will not be valid for a classical turning point, since $\lambda \to \infty$. A somewhat more refined WKB approximation formula is

$$T_l(\epsilon_\nu) = \frac{1}{1 + \exp 2G}, \tag{2.41}$$

!!! CITE PAPER !!! which still suffers from the same short-comings as the previous formula. Nevertheless, the transition amplitudes calculated with the WKB formula are generally of the right order of magnitude, which should suffice for our purposes [24].

For $\epsilon > V_{\max}$, we can no longer view the emission as tunneling, as the particle passes "over" the barrier. Instead

$$T_l = \frac{1}{1 + \exp \frac{2\pi}{\hbar\omega}(E - V_{\max})}, \tag{2.42}$$

where

$$\hbar\omega = \hbar\sqrt{\frac{1}{\mu}\left(\frac{d^2V_l}{dr^2}\right)_{r_{\max}}}. \tag{2.43}$$

!!! MAYBE NEED TRANSLATION OF SECTION OF ULLI THESIS. CAN'T FIND SOURCE !!!

$\gamma-$decay The above discription concerned the tunneling of a nucleon or cluster through a potential barrier, and is thus not applicable to gamma decay.

γ-ray strength functions f_{XL} can be used to calculate transition probabilities by γ-ray emission,

$$T_L(E) = E^{2L+1} f_{XL}(E), \tag{2.44}$$

where f_l in principle can depend on whether the transition is electric or magnetic, $X = E$ and $X = M$, respectively. Viewed experimentally, (2.44) can almost be viewed as a definition of the strength function. For exemple, the definition in the *Gamma-Ray Strength Functions* in the book *Advances in Nuclear Physics* [25], defines the strength function as

$$f^J_{ifXL} = \frac{\bar{\Gamma}_{ifXL}}{E_\gamma^{2L+1}} \rho_J(E_i), \tag{2.45}$$

and if we take f_{XL} to be independent of J and recall the definition of Γ (2.14), we find that the definitions agree up to a factor $\rho_J(E_f)/\hbar$, which is essentially a constant for a fixed final state, as considered above.

The transmission coefficient used by CODEX ... !!!TODO!!!

2.2. Finite-Range Droplet Model

The Finite-range droplet model with parameters fitted to nuclear data in 1995 [13] was used to determine the macroscopic contributions to mass excesses. The macroscopic part of the FRDM is in essence– like all macroscopic mass formulas– a refined version of the *semi-empirical mass formula* (SEMF). Just like the SEMF, the FRDM contains volume, surface, Coloumb, asymmetry (in the form of a Wigner term) and pairing terms. It also contains numerous other terms, and as such, we will not write it out here, but refer to the original literature [13].

Important to note is that our macroscopic energy was obtained for spherical nuclei, while the model parameters of the FRDM was fitted to experimental mass excesses deformations from a previous iteration, where rougher values were used for the constants. As such, our calculated macroscopic mass excesses do not contain deformation energies, and when we calculate the microscopic (pairing and shell energy), we actually calculate

$$E_{\text{exp}} - E_{\text{mac}}(\text{sphere}) = E_{\text{s+p}} + E_{\text{deformation}}, \tag{2.46}$$

which means that for deformed nuclei, our estimate of shell and pairing effects will include contributions from the deformation energy. Since the rest of the code does not take deformations into account, this is not really an additional contraint: the code cannot be expected to work for nuclei that are not close to being spherical.

The reason for this contraint is that it would be difficult to decide on which deformation parametrization to use, and which values to use for these parameters, given an N,Z, J and excitation energy. For ground states, the deformations are rougly known, as the energy in the FRDM has been minimized with respect to Nilson perturbed-spheroid parameters.

3. The Code

The CODEZ code, based on CODEX [15], contains models for the various quantities needed in statistical models. It is written to be extendable and to a large extent modular, so that the various models can easily be replaced. Details on the specific models may be found in section 2.1. To achieve this modularity, the code is written in C++ and makes use of *object-oriented* programming concepts.

The program is roughly structered as follows: Decay processes are specified by model objects, which contain models for calculating transition probabilities to possible final states. "Probabilities" here refers to $d^2P_\nu/dtdE$, roughly the probability to decay to a final state in energy interval dE during the time dt by the process ν. The probabilities need not be normalized. The model objects implement a function that for a given energy discritization tabulates a specification of the decay (The excitation energy of the final state, the spin of the final state, the particle ν which was emitted in the decay, its orbital angular momentum) along with a corresponding cummulative probability. A complete table of cummulative transition probabilities and final states is generated by looping over all model objects.

A de-excitation step may then be performed by drawing a random number between 0 and the final cummulative probability, and looking up the corresponding decay in the table. Several one-step decays from the same state may thus be performed with little extra computational costs.

The tabulation of decay probabilities, the deexcitation and the models all compile to different object-files, which are linked to produce exectable files with various purposes – such as deexciting a nucleus until its excitation energy reaches a certain value, finding the most common decay channel for several different nuclei with given excitation energies, export level densities, etc. This removes the need to excessively control the program flow in the individual main-files, which makes the code easier to read, since it mostly describes the physics – although it may lead to some code duplication.

The next section describes the individual executable programs, and demonstrates how they may be used together to solve more complicated tasks.

3.1. Programs

The CODEZ code contains three types of subprograms: programs to generate list of nuclei, programs that run on a list of nuclei, and programs that process the output of

the latter programs. The different kinds of programs may be used in a pipe, like

```
list | run | process
```

3.1.1. List generating programs

The first kind of program simply generate lists of nuclei to perform calculations for. The output of these programs are on the form illustrated by this example output:

```
#comment
*Event 1
Z11 N11 E11 J11 px11 py11 pz11
Z12 N12 E12 J12 px12 py12 pz12
*Event 2
Z21 N21 E21 J21 px21 py21 pz21
```

where Z,N,E,J,p specify the proton number, neutron number, excitation energy, spin and 3-momentum of the nucleus. If no event numbers are present, each line is assumed to be a separate event. Simpler lists could easily be written by hand, but the list-type programs make it possible to easily run a specific calculation (as specified by a "run-type" program) for a range of nuclei, or nuclei generated by a specific process.

NUCLIST

The NUCLIST program simply generates a list of nuclei for a given N, Z or A range; with a given excitation energy, spin and initial momentum. This program can be used to determine spectra from excited nuclei of certain isotopes, isobars and isotones.

Each nuclei is placed in a separate event.

QUASI

This program simulates a quasi-elastic scattering event, producing an excited prefragment as well as the participant knocked-out cluster and target fragment. The beam energy, the number of events, the participant nuclei must be specified, and the excitation energy and spin of the spectator prefragment may be specified.

The target and cluster fragments are assumed to be unexcited, which should be a good assumption for p2p reactions.

Each scattering event is placed in a separate event.

3.1.2. Programs to run on nuclei-lists

These programs can be run on a list produced by the above programs in order to perform various calculations.

SPECTRA

This program, primarily intended to be run on the output of NUCLIST, prints the probabilities of various decay modes from the initial states specified by the nuclie-list. The `-details` flag controls to which level of detail the spectra are printed. This is essentially a program to illustate the decay widths as calculated by the program, and hence it ignores event numbers.

DEEXCITE

The bulk work of an event generator is performed in this program. Each nuclei in each event in the input file is deexcited until it is below a specified threshold energy, or for a given number of deexcitation steps, and the resulting nuclei are printed to a new list, with the event number inherited from their mother nuclei. Combined with the output of QUASI and the post-processing program LIST2GUN, this program is able to act as an event generator for GEANT4 through the wrapper GGLAND.

RHO

This program produces a *tab-separated value* (tsv) file of the level density for each nuclei in the input list. By default, only the Z, N and J of the nuclei is used, and the level density is plotted for a range of excitation energies, rather than the actual energy of the nuclei in the input files, which are ignored in this mode.

POT

Like RHO, this program produces a *tab-separated value* (tsv) file for each nuclei in the input list, this time of the potential a particle has to tunnel through to be emitted by the nuclei in the list. The potential for a given particle-decay can be exported for a range of l values.

Bibliography

[1] GSI - R3B, 2014. `https://www.gsi.de/work/forschung/nustarenna/nustarenna_divisions/kernreaktionen/activities/r3b.htm`. (accessed 2015-04-16).

[2] J. J. Gaimard and K. H. Schmidt. A reexamination of the abrasion-ablation model for the description of the nuclear fragmentation reaction. *Nuclear Physics A*, 531(3), 1991.

[3] J. Bowman, W. Swiatecki, and C. Tsang. *Abrasion and ablation of heavy ions*. Jul 1973. http://www.osti.gov/scitech/servlets/purl/4259977.

[4] N. Metropolis, R. Bivins, M. Storm, et al. Monte Carlo Calculations on Intranuclear Cascades. I. Low-Energy Studies. *Phys. Rev.*, 110:185–203, Apr 1958. http://link.aps.org/doi/10.1103/PhysRev.110.185.

[5] F. Cucinotta, J. Wilson, J. Shinn, and R. Tripathi. Assessment and requirements of nuclear reaction databases for {GCR} transport in the atmosphere and structures. *Advances in Space Research*, 21(12):1753 – 1762, 1998. http://www.sciencedirect.com/science/article/pii/S0273117798000623.

[6] A. Goldhaber. Statistical models of fragmentation processes. *Physics Letters B*, 53(4):306 – 308, 1974. http://www.sciencedirect.com/science/article/pii/0370269374903888.

[7] K. H. Schmidt and W. Morawek. The conditions for the synthesis of heavy nuclei. *Reports on Progress in Physics*, 54(7), 1991.

[8] K. Krane. *Introductory Nuclear Physics*, chapter Nuclear Fission. Wiley, 1987.

[9] W. J. Swiatecki. NOTE ON NUCLEAR DISINTEGRATION WIDTHS. *Australian Journal of Physics*, 36(5):641–647, 1983.

[10] Wolfram Research, Inc. . Number of partitions of an integer into distinct parts: Introduction to partitions, 2015. http://functions.wolfram.com/IntegerFunctions/PartitionsQ/introductions/Partitions/ShowAll.html (accessed 2015-05-20).

[11] International Atomic Energy Agency. *Handbook for calculations of nuclear reaction data, RIPL-2*, chapter Nuclear Level Densities. 2006.

[12] T. Ericson. The statistical model and nuclear level densities. *Adv.Phys.*, 9:425–511, 1960.

[13] P. Moller, J. Nix, W. Myers, and W. Swiatecki. Nuclear Ground-State Masses and Deformations. *Atomic Data and Nuclear Data Tables*, 59(2):185 – 381, 1995. http://www.sciencedirect.com/science/article/pii/S0092640X85710029.

[14] M. Grossjean and H. Feldmeier. Level density of a Fermi gas with pairing interactions. *Nuclear Physics A*, 444(1):113 – 132, 1985. http://www.sciencedirect.com/science/article/pii/0375947485902945.

[15] U. Gollerthan. Untersuchungen zur Emission geladener Teilchen bei der kalten Fusion von $^{90}\mathrm{Zr} + {}^{89}\mathrm{Y}$. Master's thesis, Technische Hochschule Darmstadt, 1988.

[16] J. Błocki, J. Randrup, W. Świątecki, and C. Tsang. Proximity forces. *Annals of Physics*, 105(2):427 – 462, 1977. http://www.sciencedirect.com/science/article/pii/0003491677902494.

[17] C. D. Fosco, F. C. Lombardo, and F. D. Mazzitelli. An improved proximity force approximation for electrostatics. *Annals Phys.*, 327:2050–2059, 2012.

[18] C. D. Fosco, F. C. Lombardo, and F. D. Mazzitelli. The proximity force approximation for the Casimir energy as a derivative expansion. *Phys.Rev.*, D84:105031, 2011.

[19] I. Dutt and R. K. Puri. Comparison of different proximity potentials for asymmetric colliding nuclei. *Phys.Rev.*, C81:064609, 2010.

[20] M. Balasubramaniam and N. Arunachalam. Proton and α-radioactivity of spherical proton emitters. *Phys. Rev. C*, 71:014603, Jan 2005. http://link.aps.org/doi/10.1103/PhysRevC.71.014603.

[21] H. F. Zhang, Y. J. Wang, J. M. Dong, J. Q. Li, and W. Scheid. Concise methods for proton radioactivity. *Journal of Physics G: Nuclear and Particle Physics*, 37(8):085107–085107, 2010.

[22] W. D. Myers. Geometric properties of leptodermous distributions with applications to nuclei. *Nuclear Physics A*, 204(3):465 – 484, 1973. http://www.sciencedirect.com/science/article/pii/0375947473903886.

[23]

[24] C.-S. Ng. WKB - Not So Bad After All. *ArXiv e-prints*, June 2011.

[25] M. Baranger and E. Vogt. *Advances in Nuclear Physics: Volume 7*, chapter Gamma-Ray Strength Functions. Springer US, Boston, MA, 1973.

A. Appendix 1

B. Code

```
struct spec_POS_t
{
  SPEC_FLOAT(_dx,              2.5,"cm","full width x of active volume")
      ;
  SPEC_FLOAT(_dy,              2.5,"cm","full width y of active volume")
      ;
  SPEC_FLOAT(_dz,           0.03,"cm","full width z of active volume");
  SPEC_FLOAT(_lgheight,      2,"cm","lightguide height over active
      volume");
  SPEC_FLOAT(_lgheadd,      0.70,"cm","size of square-shaped lightguide-
      heads");
  SPEC_MEDIA(_type,    "plastic",""   ,"POS active volume material.");
  SPEC_MEDIA(_lgtype, "plastic",""   ,"Lightguide material");
};
```

```
#include "auto_gen/spec_info_pos.hh"

#define UNUSED_PARAM(x)
```

This function is called when GGLAND creates the detector.

```
gg_geom_obj *make_POS(void *vspec,uint32_t UNUSED_PARAM(mask_set)
                      ,const transform_matrix *loc_rot
                      ,det_name_no_info *name_no)
{
```

C. Svenska här